

## Single-crystal analysis of La-doped pyromorphite [Pb<sub>5</sub>(PO<sub>4</sub>)<sub>3</sub>Cl]

JULIA SORDYL<sup>1,2,\*</sup>, JOHN RAKOVAN<sup>3</sup>, PETER C. BURNS<sup>4,5,†</sup>, JUSTYNA TOPOLSKA<sup>1</sup>, ADAM WŁODEK<sup>1</sup>,  
JENNIFER E.S. SZYMANOWSKI<sup>4</sup>, GINGER E. SIGMON<sup>4</sup>, JAROSŁAW MAJKA<sup>1,2,‡</sup>, AND MACIEJ MANECKI<sup>1,2</sup>

<sup>1</sup>Faculty of Geology, Geophysics and Environmental Protection, AGH University of Science and Technology, al. Mickiewicza 30, 30-059 Kraków, Poland

<sup>2</sup>Department of Earth Sciences, Uppsala University, Villavägen 16, SE-752 36 Uppsala, Sweden

<sup>3</sup>New Mexico Bureau of Geology & Mineral Resources New Mexico Institute of Mining & Technology, Socorro, New Mexico 87801-4796, U.S.A.

<sup>4</sup>Department of Civil and Environmental Engineering and Earth Sciences, University of Notre Dame, Notre Dame, Indiana 46556, U.S.A.

<sup>5</sup>Department of Chemistry and Biochemistry, University of Notre Dame, Notre Dame, Indiana, 46556, U.S.A.

### ABSTRACT

Rare earth elements (REE) in calcium apatite have been widely described in the literature. Based on the investigations of minerals and their synthetic analogs, the mechanism of substitution of REE<sup>3+</sup> for Ca<sup>2+</sup> and their structural positions are well established. Although the presence of REE in natural pyromorphite has been reported, the structural response of substitution of REE<sup>3+</sup> for Pb<sup>2+</sup> is not established. A better understanding of REE-rich Pb-apatite may facilitate the potential use of this mineral in industrial processes. Two La-doped pyromorphite analogs [Pb<sub>5</sub>(PO<sub>4</sub>)<sub>3</sub>Cl] and two control pyromorphite analogs (with the absence of La) were synthesized from aqueous solutions at 25 °C. Na<sup>+</sup> and K<sup>+</sup> were used as charge-compensating ions to facilitate the incorporation of trivalent REE cations (La<sup>3+</sup> + Na<sup>+</sup> ↔ 2Pb<sup>2+</sup> and La<sup>3+</sup> + K<sup>+</sup> ↔ 2Pb<sup>2+</sup>). Microprobe analysis, scanning electron microscopy, and Raman spectroscopy were used to confirm the purity of obtained phases. High-precision crystal structure refinements (R<sub>1</sub> = 0.0140–0.0225) of all four compounds were performed from single-crystal X-ray diffraction data. The La content varied from 0.12(1) to 0.19(1) atoms per formula unit with the counter ions of K<sup>+</sup> and Na<sup>+</sup>, respectively. Both substituting ions were accommodated at the Pb1 site only. By comparing the La-doped pyromorphite analogs with their control samples, it was possible to detect small changes in bond distances and polyhedral volumes caused by the La substitution. Variations in individual and mean interatomic distances reflected the cumulative effect of both the amount of substitution and ionic radii of substituting ions (La<sup>3+</sup>, Na<sup>+</sup>, and K<sup>+</sup>).

**Keywords:** Apatite, pyromorphite, crystal structure, rare earth elements

### INTRODUCTION

Pyromorphite [Pb<sub>5</sub>(PO<sub>4</sub>)<sub>3</sub>Cl] belongs to the apatite supergroup of minerals and occurs in the oxidation zone of polymetallic deposits (Pasero et al. 2010). The pyromorphite structure was discussed in detail in Dai and Hughes (1989) and Okudera (2013). In the unit cell, Pb occupies four Pb1 sites (bonding to nine O atoms: 3 × O1, 3 × O2, and 3 × O3) and six Pb2 sites (bonding to six O atoms [O1, O2, and 4 × O3] and two Cl atoms located on the hexad at 0,0,0 and 0,0,1/2). Two distinct Pb polyhedrons are linked through O atoms shared with phosphate tetrahedra and are hexagonally distributed about a central [001] anion column.

As Pb-phosphates are highly stable under environmental conditions found in the critical zone of the Earth (Nriagu 1974), pyromorphite is a natural weathering product in Pb-contaminated soils and a product of in situ immobilization by precipitation induced by phosphate amendments (Laperche et al. 1997; Ma et al. 1993, 1995; Manecki et al. 2000, 2020; Tang et al. 2013; Manecki 2019). The presence of rare earth elements (REE) has


been reported in natural pyromorphite (Markl et al. 2014). However, the mechanisms of incorporation of REE, their structural position in Pb-apatite, and charge compensation mechanisms are poorly understood, as compared to widely described calcium apatite (Borisov and Klevcova 1963; Mackie and Young 1973; Hughes et al. 1991; Fleet and Pan 1995, 1997a, 1997b; Rakovan and Reeder 1996; Fleet et al. 2000). This is because the REE content in Ca-apatite plays a role in petrological and genetic interpretations of mineral deposit formation and petrogenesis (Papike et al. 1984; Sha and Chappell 1999; Belousova et al. 2002; Harlov 2015; Bouzari et al. 2016; Jonsson et al. 2016; O’Sullivan et al. 2018; Andersson et al. 2019; Zhang et al. 2021). Nevertheless, the presence of REE in Pb-apatite is of interest because of its potential use in industrial processes.

Laboratory experiments for the synthesis of Pb-apatite analogs containing REE were described by Newby (1981) in an unpublished Ph.D. dissertation, which demonstrated differences in the amount of incorporated REE under different pH conditions. Owing to the similarity in their structures (White et al. 2005), the substitution mechanisms of REE in Ca- and Pb-apatites are likely to exhibit similarities. However, given the larger unit-cell size and the different preference of Pb over Ca in occupying the cationic position, as well as the presence of a free electron pair on

\* E-mail: sordyl@agh.edu.pl. Orcid 0000-0002-5772-5200

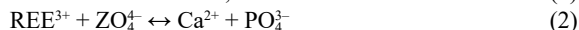
† Orcid 0000-0002-2319-9628

‡ Orcid 0000-0002-6792-6866

 Open access: Article available to all readers online.

the  $\text{Pb}^{2+}$  ion (Kim et al. 2000; Baikie et al. 2014), the mechanism and magnitude of substitution may be different.

Exchange of  $\text{REE}^{3+}$  for  $\text{Ca}^{2+}$  requires a coupled substitution. The two most common mechanisms of REE substitution in Ca, P-bearing apatite supergroup members are (Rønsbo 1989; Pan and Fleet 2002):



In natural Ca-apatites,  $\text{Me}^+$  is most frequently Na, and  $\text{ZO}_4^-$  is most often  $\text{SiO}_4$ .

In this study, pyromorphite  $\text{Pb}_5(\text{PO}_4)_3\text{Cl}$  was chosen as the model Pb-apatite, and La was chosen as the model REE, as its chemical and physical properties well represent the entire group of light rare earth elements. Moreover, it is easily available in high-purity reagent form for synthesis [ $\text{La}(\text{NO}_3)_3 \cdot 6\text{H}_2\text{O}$ ].  $\text{Na}^+$  and  $\text{K}^+$  were used as model charge-compensating ions. It was hypothesized that the substitution occurs through the following reactions:



The research methodology involved the synthesis of pyromorphite crystals from aqueous solutions, which is most relevant to natural environmental conditions and to natural REE-enriched pyromorphite found in the oxidation zones of deposits. Therefore, in the present study, we report a single-crystal X-ray diffraction study of four synthetic  $\text{Pb}_5(\text{PO}_4)_3\text{Cl}$  pyromorphite analogs containing La and Na or La and K substitutions and control samples synthesized from aqueous solutions under the same conditions in the absence of La. The synthesized samples were characterized using scanning electron microscopy (SEM), microprobe analysis, Raman spectroscopy, and single-crystal X-ray diffraction. We aimed to provide an explanation of the site occupancy and substitution mechanism, to determine the effect of  $\text{Na}^+$  and  $\text{K}^+$  substitution on the magnitude of  $\text{La}^{3+}$  substitution, and to capture similarities and differences with the better-studied Ca-apatite. Our findings contribute to a better understanding of light REE substitution in Pb-apatite, which is particularly important because REE are considered critical metals and REE-rich Pb-apatite may prove to be useful in future industrial applications.

## EXPERIMENTAL PROCEDURE

Four pyromorphite analogs were synthesized via precipitation from aqueous solution at room temperature, namely two La-doped samples:  $\text{La}_x\text{Na}_x\text{Pb}_{5-2x}(\text{PO}_4)_3\text{Cl}$  (La-Na-Pym),  $\text{La}_x\text{K}_x\text{Pb}_{5-2x}(\text{PO}_4)_3\text{Cl}$  (La-K-Pym), and two control samples without La:  $\text{Na}_{2x}\text{Pb}_{5-x}(\text{PO}_4)_3\text{Cl}$  (Na-Pym) and  $\text{K}_{2x}\text{Pb}_{5-x}(\text{PO}_4)_3\text{Cl}$  (K-Pym). The starting mixtures of  $\text{Pb}(\text{NO}_3)_2$  with  $\text{La}(\text{NO}_3)_3 \cdot 6\text{H}_2\text{O}$  in a molar proportion of 4:1 (or without  $\text{La}(\text{NO}_3)_3 \cdot 6\text{H}_2\text{O}$  for control samples) were dissolved in double-distilled water and added slowly (10 mL/h) by dripping through a glass funnel into the still solution column of dissolved  $\text{PO}_4^{3-}$  and  $\text{Cl}^-$  salts:  $\text{NaH}_2\text{PO}_4 \cdot 6\text{H}_2\text{O}$  and  $\text{NaCl}$  for La-Na-Pym and Na-Pym;  $\text{K}_2\text{HPO}_4$  and  $\text{KCl}$  for La-K-Pym and K-Pym. In all the experiments, the largest crystals were needle-shaped (up to 1 mm long) and precipitated at the end of the funnel. These crystals were collected using tweezers, washed with double-distilled water, and examined via SEM in low vacuum for the uncoated samples using an FEI Quanta 200 FEG SEM (Hillsboro, Oregon U.S.A.) equipped with secondary-electron and backscattered-electron detectors. Energy-dispersive spectrometry (EDS, FEI Quanta, Lausanne, Switzerland) was employed to evaluate possible variations in chemical composition.

Quantitative chemical analyses were performed via electron microprobe

(EMP) analysis using a JEOL SuperProbe JXA-8230 located at the Laboratory of Critical Elements at the Faculty of Geology, Geophysics and Environmental Protection, AGH UST Krakow. The EMP operated at an accelerating voltage of 15 kV, a probe current of 15 nA, a peak count time of 20 s, and background count time of 10 s, with a beam diameter of 1–5  $\mu\text{m}$ , depending on individual crystal sizes. Standards [analytical lines and wavelength-dispersive spectrometry (WDS) diffracting crystals] included fluorite for F ( $K\alpha$ , LDE1), fluorapatite for P ( $K\alpha$ , PET), albite for Na ( $K\alpha$ , TAP) and Si ( $K\alpha$ , TAP), sanidine for K ( $K\alpha$ , PET), crocoite for Pb ( $M\alpha$ , PET) tugtupite for Cl ( $K\alpha$ , PET), and synthetic  $\text{LaPO}_4$  phosphate for La ( $L\alpha$ , LiF) (Jarosewich and Boatner 1991). Durango apatite was used as secondary reference material for monitoring the Cl analysis. Fluorapatite was not used as the F reference material because of time-dependent orientation effects of fluorapatite on the X-ray emission. During EMP measurement of the  $\text{NaK}\alpha$ ,  $\text{KK}\alpha$ , and  $\text{ClK}\alpha$  lines of all synthetic Pb-apatite crystals, no time-dependent intensity loss effects were recorded. For sample preparation, a dry precipitate was mixed with epoxy resin, placed in a standard ring, and polished.

A Thermo Scientific DXR Raman confocal microscope was used to collect Raman spectra of samples, which were excited with a green laser (532 nm, with a power maintained at 10 mW and a slit aperture of 50  $\mu\text{m}$ ) in the range of 100–3580  $\text{cm}^{-1}$ . Deconvolution of spectra was done using OMNIC for Dispersive Raman software (Thermo Fisher Scientific) in the ranges of 350–600 and 800–1200  $\text{cm}^{-1}$  using the Gaussian/Lorentzian function, high-sensitivity factor, and a constant baseline.

Single-crystal X-ray diffraction measurements were performed on a Bruker APEXII Quazar CCD X-ray diffractometer with  $\text{MoK}\alpha$ ,  $\lambda = 0.71073 \text{ \AA}$ , for two control samples (Na-Pym and K-Pym) at 273 K. A Rigaku XtaLAB Synergy-S diffractometer equipped with a full 4-circle kappa goniometer, a HyPix6000E detector (hybrid), and  $\text{MoK}\alpha$  X-ray radiation from a microfocus sealed tube was used for collection of the X-ray diffraction data at 180 K for La-doped samples (La-Na-Pym and La-K-Pym). One sample (La-K-Pym) was analyzed at both temperatures, 273(2) and 180(2) K, showing that final parameters did not change significantly due to cooling (Online Materials' Appendix A). The results of the measurements at these two temperatures are the same within the experimental error. The reason for the absence of thermal expansion in this temperature range is unknown. It is possible, though, that in a larger range of temperatures such a tendency would be observed. According to previous studies for Pb-apatite, pure pyromorphite shows thermal expansion in the temperature range 298–1373 K (Hovis et al. 2015; Knyazev et al. 2015; Gu et al. 2020). However, there is no similar data for REE-substituted pyromorphite. The La-Na-Pym sample was measured only at 180 K. A data collection strategy was calculated with the CrysAlis<sup>Pro</sup> software. The crystal structures were refined using the Bruker SHELXTL v.6.14 package of programs (Sheldrick 2015).

## RESULTS AND DISCUSSION

### Morphology of the crystals

La-doped samples yielded elongated needle-like crystals with hexagonal cross sections in the size range of 100–500  $\mu\text{m}$  (Figs. 1a and 1b), whereas those containing no La yielded two generations of crystals: needle-like crystals elongated parallel to the [001] of 200  $\mu\text{m}$  and hexagonal rods of <10  $\mu\text{m}$  (Figs. 1c and 1d). EDS and microprobe analyses confirmed the intended chemical compositions for both types of crystals habit.

### Chemistry

Chemical compositions of each phase were analyzed using 13–21 individual spots. For each sample, two results with totals furthest from 100% were discarded. Therefore, the calculation of the chemical formulas was based on the average of the 11–18 superior spot analyses for each sample. The microprobe analysis results (Table 1) showed that the average  $\text{La}_2\text{O}_3$  concentrations were 1.19 wt% ( $\sigma = 0.68$ ) and 0.63 wt% ( $\sigma = 0.28$ ) for La-Na-Pym and La-K-Pym, respectively. The relatively high standard deviations may be attributed to heterogeneity among different crystals.

Owing to the difficulties in the preparation of small crystals, there were several problems in the quantitative analysis of the chemical composition, mainly in the determination of the Cl

content in small or porous crystals (due to the crystal habit). The epoxy infiltrated porosity, causing an artificial Cl content within the samples. Crystal structure refinement, as discussed below, confirmed no vacancies at the column anion X-site. Furthermore, no other monovalent anions were available in the system, and Raman spectroscopy did not reveal the presence of OH in the samples (Fig. 2). This indicates that the X-site is fully occupied by the Cl<sup>-</sup>. Therefore, we interpret EMP data that yield Cl concentrations different from 1 apfu suspect.

Quantitative analysis of Na<sub>2</sub>O and K<sub>2</sub>O in Pb-rich apatite (the average amount of PbO in all samples is 80.2 wt%) was also challenging due to the low contents of these in the pyromorphites and the molar mass differences between the Pb and Na or K ions. The inconsistency of Na and K contents between WDS and structure refinement likely results from the detection limit of the electron microprobe analysis under the conditions applied. Therefore, all average empirical formulas based on electron microprobe analysis exhibit slight cation deficiency in charge balance.

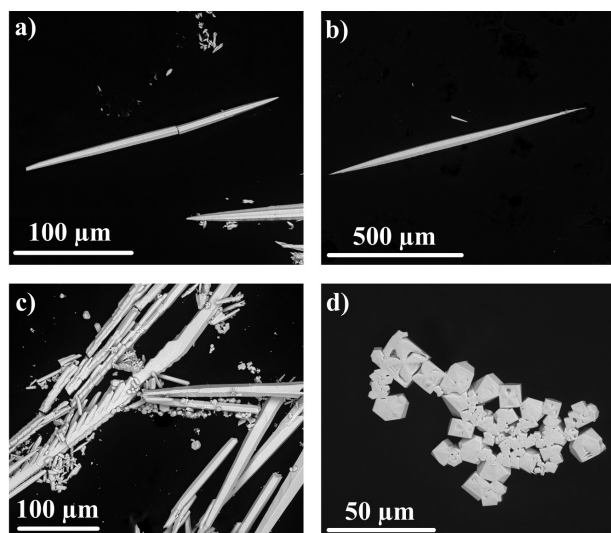


FIGURE 1. Scanning electron micrographs (BSE) of synthesized analogs: (a) La-Na-Pym; (b) La-K-Pym; (c) control Na-Pym; and (d) control K-Pym.

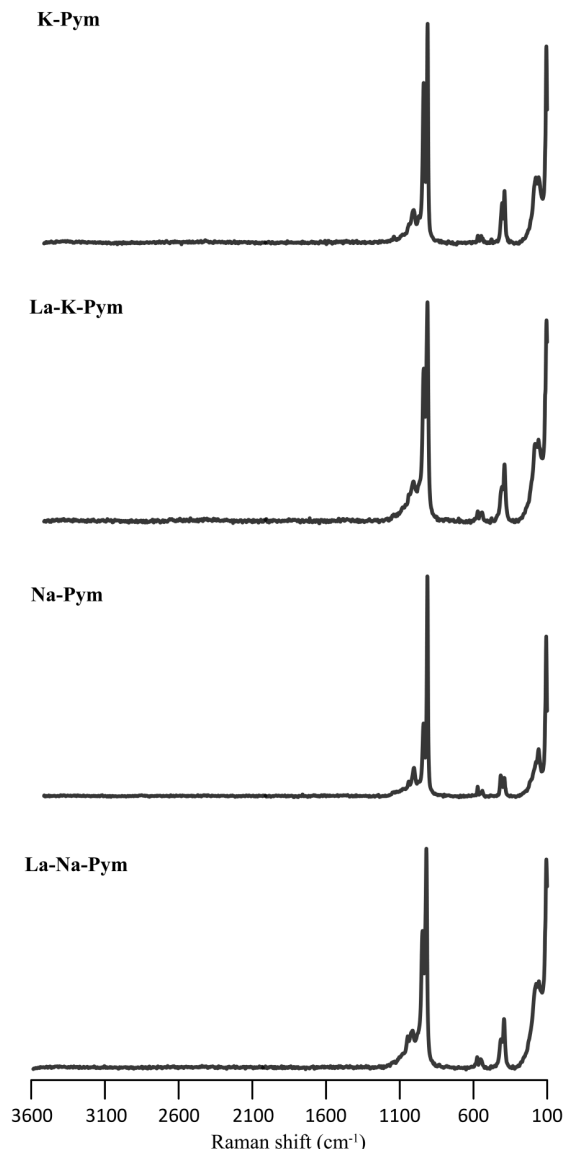


FIGURE 2. Raman spectra of synthesized analogs of La-doped pyromorphites and control samples in the 100–3600 cm<sup>-1</sup> region.

TABLE 1. Wavelength-dispersive analyses for all analyzed samples (see Online Materials<sup>1</sup> Appendix B for all WDS data)

	La-Na-Pym [wt%]	Na-Pym [wt%]	La-K-Pym [wt%]	K-Pym [wt%]
P <sub>2</sub> O <sub>5</sub>	16.03(24)	15.63(37)	15.53(27)	15.41(41)
PbO	79.42(90)	81.27(71)	79.20(58)	81.09(51)
Na <sub>2</sub> O	0.04(4)	0.02(4)	b.d.	b.d.
K <sub>2</sub> O	b.d.	b.d.	0.05(9)	0.03(3)
La <sub>2</sub> O <sub>3</sub>	1.19(68)	b.d.	0.63(28)	b.d.
Cl	2.34(19)	2.61(20)	2.97(24)	2.96(24)
O=Cl	-0.53	-0.59	-0.67	-0.67
Total	98.49	98.94	97.69	98.82
<b>apfu based upon 13 anions</b>				
P	3.03(1)	3.01(2)	3.01(2)	2.99(3)
Pb	4.77(9)	4.97(6)	4.88(7)	5.01(8)
Na	0.02(2)	0.01(2)	b.d.	b.d.
K	b.d.	b.d.	0.01(3)	0.01(1)
La	0.10(6)	b.d.	0.05(2)	b.d.
Cl	0.89(8)	1.01(9)	1.15(10)	1.15(10)
Empirical formula	Pb <sub>4.77(9)</sub> La <sub>0.10(6)</sub> Na <sub>0.02(2)</sub> (PO <sub>4</sub> ) <sub>3.03(1)</sub> Cl <sub>0.89(8)</sub>	Pb <sub>4.97(6)</sub> Na <sub>0.01(2)</sub> (PO <sub>4</sub> ) <sub>3.01(2)</sub> Cl <sub>1.01(9)</sub>	Pb <sub>4.88(7)</sub> La <sub>0.05(2)</sub> K <sub>0.01(3)</sub> (PO <sub>4</sub> ) <sub>3.01(2)</sub> Cl <sub>1.15(10)</sub>	Pb <sub>5.01(8)</sub> K <sub>0.01(1)</sub> (PO <sub>4</sub> ) <sub>2.99(3)</sub> Cl <sub>1.15(10)</sub>

Note: b.d. = below detection.

### Purity confirmation by Raman spectroscopy

The aim of this study was the structural analysis of La-doped pyromorphite free from impurities such as carbonate or hydroxyl ions. Therefore, to verify the absence of potential impurities of  $\text{CO}_3^{2-}$  or  $\text{OH}^-$ , Raman spectroscopy was the method of choice. The Raman spectra of all phases in the range of 100–3600  $\text{cm}^{-1}$  are shown in Figure 2, and the described vibrational modes in the range of 100–1200  $\text{cm}^{-1}$  are shown in Figure 3.

The carbonate ion can be incorporated into an apatite structure in three positions: as a substitution for the anion in the hexagonal channel (two type-A substitutions) and for  $\text{PO}_4^{3-}$  tetrahedron (type-B substitution) (Fleet et al. 2004). The quantity of carbonate ions in the apatite structure depends mainly on the chemical composition and the conditions of synthesis (Vignoles et al. 1988). The maximum content of carbonates in synthetic lead apatite precipitated from an aqueous solution does not exceed 2.25 wt% (Kwaśniak-Kominek et al. 2017). The carbonate bands are found in the Raman spectra of pyromorphite at around 1116  $\text{cm}^{-1}$  (Botto et al. 1997). In carbonated hydroxylpyromorphite,  $\text{Pb}_5(\text{PO}_4)_3(\text{OH})$ , this band is located at 1102  $\text{cm}^{-1}$  (Kwaśniak-Kominek et al. 2017) and is attributed to  $\nu_1 \text{CO}_3^{2-}$ . No such bands or other Raman bands attributable to carbonate were observed. This indicates the absence of carbonate in the structures of the synthetic pyromorphites. In addition, Raman scattering was not observed above 1200  $\text{cm}^{-1}$  (Fig. 2), indicating the absence of  $\text{OH}^-$  groups.

In the pyromorphite spectra, the most intense bands at 919–947  $\text{cm}^{-1}$  along with the bands in the 974–1048  $\text{cm}^{-1}$  region are attributed to the stretching vibrations of the P–O bond ( $\nu_1$  and  $\nu_3$ ) (Levitt and Condrate 1970; Bartholomäi and Klee 1978; Botto et al. 1997; Frost and Palmer 2007; Bajda et al. 2011). A very weak band was apparent in all deconvoluted spectra at 1091 or 1092  $\text{cm}^{-1}$ , which may simply be a part of the background or the result of degeneration of the Pb-apatite structure (Kwaśniak-Kominek et al. 2017). The bands in the 541–586  $\text{cm}^{-1}$  region correspond to the  $\nu_4$  scissor vibrations of the O–P–O angle and may be resolved into three bands for control pyromorphites, and into four bands for La-doped pyromorphites. Splitting was also observed for the  $\nu_2$  scissor vibrations of the O–P–O angle in the 392–439  $\text{cm}^{-1}$  region. These, however, were not systematic, as the bands for control samples were split into three bands and those for La-doped pyromorphites into two (La-Na-Pym) or four (La-K-Pym). Such splitting is attributed to the reduction of the symmetry of the ideal  $(\text{PO}_4)^{3-}$  tetrahedron (Adler 1964). A broad profile from 100 to 250  $\text{cm}^{-1}$  was attributed to lattice vibrations. However, the presence or absence of the strongest band at 107  $\text{cm}^{-1}$  is strongly related to the crystal orientation. Therefore, the lattice vibrations are of little use for phase identification. All band positions resolved in the spectra collected for pyromorphite crystals are consistent with the previously described Raman spectra for pyromorphite (Levitt and Condrate 1970; Bartholomäi and Klee 1978; Botto et al. 1997; Frost and Palmer 2007; Bajda et al. 2011). Owing to the small amount of La substituting for Pb, no significant shifts were observed in the positions of the bands for doped samples. However, the intensities of the different bands varied. This is influenced by the crystal orientation relative to the incident beam (Frost and Palmer 2007).

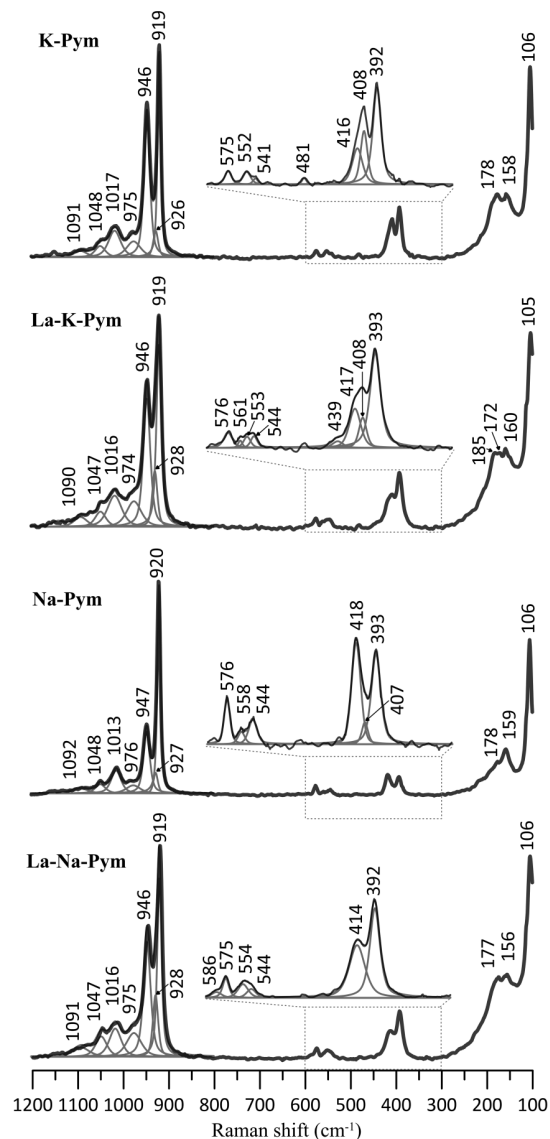


**FIGURE 3.** Raman spectra of synthesized analogs of La-doped pyromorphites and control samples in the 100–1200  $\text{cm}^{-1}$  region with deconvoluted phosphate bands at the 300–600 and 800–1100  $\text{cm}^{-1}$  regions.

### Structure

**Refinement of the structure.** The crystallographic characteristics and conditions for data collection are shown in Table 2. The crystallographic information files (CIF) can be found in the Online Materials' Appendix C. Crystal structures were solved and refined in space group  $P6_3/m$ . No reflections characteristic of a monoclinic superstructure were noted (Mackie et al. 1972; Elliott et al. 1973; Bauer and Klee 1993). All structures were refined to  $R1 = 0.0140$ – $0.0225$ . The positional parameters, equivalent isotropic displacement parameters, and site occupancies can be found in Online Materials' Appendix D.

**Site occupancy.** In all the refined structures, the Pb2, P, and Cl sites were fully occupied by a single constituent. However, the

**TABLE 2.** Experimental details and crystallographic characteristics of the analyzed samples

	La-Na-Pym	Na-Pym	La-K-Pym	K-Pym
Diffractometer	Rigaku Oxford Diffraction	Bruker AXS	Rigaku Oxford Diffraction	Bruker AXS
X-ray radiation		MoK $\alpha$ ( $\lambda = 0.71073 \text{ \AA}$ )		
Temperature (K)	180(2)	273(2)	180(2)	273(2)
Space group			<i>P6<sub>3</sub>/m</i>	
Unit-cell parameters				
<i>a</i> ( $\text{\AA}$ )	9.98367(9)	9.996(2)	10.00129(8)	9.9944(4)
<i>c</i> ( $\text{\AA}$ )	7.30631(10)	7.319(2)	7.29865(8)	7.3142(4)
<i>V</i> ( $\text{\AA}^3$ )	630.679(14)	633.3(3)	632.244(12)	632.72(6)
<i>Z</i>	2	2	2	2
Absorption coefficient ( $\text{mm}^{-1}$ )	66.522	66.225	64.024	66.303
<i>F</i> (000)	1035	1129	1113	1130
$\theta$ range	2.36 to 29.03°	2.35 to 29.01°	2.35 to 33.78°	2.35 to 28.95°
Index ranges	-13 < = <i>h</i> < = 13, -13 < = <i>k</i> < = 13, -9 < = <i>l</i> < = 9,	-13 < = <i>h</i> < = 13 -13 < = <i>k</i> < = 12, -9 < = <i>l</i> < = 9	-15 < = <i>h</i> < = 15, -15 < = <i>k</i> < = 15, -10 < = <i>l</i> < = 11	-13 < = <i>h</i> < = 13, -13 < = <i>k</i> < = 13, -9 < = <i>l</i> < = 9
Collected reflections/unique reflections	43286/591	7606/593	45590/893	15516/586
Refinement method		Full-matrix least-squares on <i>F</i> <sup>2</sup>		
Refined parameters	41	42	43	41
<i>R</i> 1, <i>F</i> <sub>o</sub> > 4 $\sigma$ ( <i>F</i> <sub>o</sub> )	0.0140	0.0215	0.0225	0.0196
<i>R</i> 1, all unique data	0.0149	0.0222	0.0238	0.0201
<i>wR</i> 2	0.0285	0.0509	0.0448	0.0432
Goof	1.194	1.214	1.189	1.205
Extinction coefficient	0.00021(6)	0.00102(14)	0.00006(7)	0.00018(8)
Largest difference peaks ( $e^{-\text{\AA}^{-3}}$ )	1.476 and -0.802	2.831 and -1.093	4.679 and -1.960	2.829 and -1.008

scattering from the Pb1 site indicated the substitution of lighter elements. Based on this, the La, K, and Na ions were assigned exclusively to the Pb1 site. The occupancies were refined with the constraints of  $\text{Pb1} + \text{La} + \text{X} = 1$  ( $\text{X} = \text{Na}$  or  $\text{K}$ ) for La-doped samples and  $\text{Pb1} + \text{X} = 1$  for control samples. The following chemical formulas were derived from the refinements:  $\text{Pb}_{4.62(1)}\text{La}_{0.19(1)}\text{Na}_{0.19(1)}(\text{PO}_4)_3\text{Cl}$  (La-Na-Pym),  $\text{Pb}_{4.76(1)}\text{La}_{0.12(1)}\text{K}_{0.12(2)}(\text{PO}_4)_3\text{Cl}$  (La-K-Pym),  $\text{Pb}_{4.90(3)}\text{Na}_{0.10(4)}(\text{PO}_4)_3\text{Cl}$  (Na-Pym), and  $\text{Pb}_{4.88(3)}\text{K}_{0.12(4)}(\text{PO}_4)_3\text{Cl}$  (K-Pym). Small deficiencies in positive charge are probably easily compensated by vacancies among anionic positions, which are below the detection limit of the structural and microprobe analysis.

Various structural studies of La-doped apatites have been reported (Cockbain and Smith 1967; Mayer et al. 1980; Mayer and Swissa 1985; Hughes et al. 1991; Fleet et al. 2000). The site preference for La is strongly related to the chemical composition of apatite. In an X-ray study of a synthetic lanthanum calcium silicate apatite  $\text{Ca}_4\text{La}_6(\text{SiO}_4)_6(\text{OH})_2$  (space group *P6<sub>3</sub>/m*), Cockbain and Smith (1967) concluded that the La atoms are randomly distributed between the two Ca sites. Hughes et al. (1991) described the observed site preference of light REE for the Ca2 site based on the single-crystal analysis of four natural apatites,  $\text{Ca}_5(\text{PO}_4)_3(\text{F},\text{OH})$ , with REE substitutions (space group *P6<sub>3</sub>/m*). In contrast, the Ca1 site is favored to host La in the structure of chlorapatite,  $\text{Ca}_5(\text{PO}_4)_3\text{Cl}$  (Fleet et al. 2000). In this case, the substitution of Cl for (F, OH) results in the distortion and large increase in size of the  $\text{Ca}_2\text{O}_6\text{X}$  polyhedron, which is consistent with this unusual Ca-apatite site preference. However, these crystals of REE-doped chlorapatite were monoclinic with the space group *P2<sub>1</sub>/b*. Numerous studies on REE-doped Ca-apatite have shown that the volatile anion components (F, OH, Cl) are a significant factor in the selectivity of apatite for REE. This is due to their marked influence on the stereochemical environment and the effective size of the Ca2 site (Fleet and Pan 1997b).

The first attempts to refine the site preference of light REE in Pb-bearing apatite were made by Mayer et al. (1980) and Mayer and Swissa (1985). Their conclusions, however, were based only

on the lattice parameter changes, mainly the *c/a* ratios, calculated from X-ray powder data. They described some structural differences in F- and Cl-end-members that potentially led to different site preferences for La, but in all cases, La preference for Pb1 was observed. Partial ordering was noted, i.e., the Pb ions mainly occupied the 6*h* position (Pb2 site), while the smaller rare earth cations occupied in the 4*f* column positions (Pb1 site). These findings are consistent with our refinements. Pb has a strong preference for the Me(2) (6*h*) site in the apatite structure because it better accommodates the stereoactive 6*s*<sup>2</sup> electron lone pair on the Pb<sup>2+</sup> cation. Moreover, the avoidance of the Me2 site by REE in Cl-bearing apatite is caused by the off-centering of Pb at the Me2 site, helped by the Cl at the channel. Therefore, the Me1 (4*f*) site is more susceptible to substitution of other ions (Rouse et al. 1984). Similar preferences were found in Pb-substituted hydroxylapatite,  $\text{Ca}_5(\text{PO}_4)_3(\text{OH})$ , phosphohedyphane,  $\text{Ca}_2\text{Pb}_3(\text{PO}_4)_3\text{Cl}$ , and fluorphosphohedyphane,  $\text{Ca}_2\text{Pb}_3(\text{PO}_4)_3\text{F}$  (Bigi et al. 1991; Kampf et al. 2006; Kampf and Housley 2011), where Pb<sup>2+</sup> always fills the Me2 site first.

Bond-valence calculations for the substitution of La and Na (or K) for Pb are either inconclusive or not fully consistent with the structural findings (Table 3). Based on the bond valence-sum rule, La<sup>3+</sup> should prefer the Pb2 site. However, in the case of apatite, ambiguity may occur in the interpretation of bond valence: calculations of bond valence values are based on the relationship between bond distance and bond strength and include a component attributed to variation in the size of structural positions that can cause ambiguity in interpretation (Fleet and Pan 1995).

**Structure variation.** Table 4 shows the variations in selected bond lengths, bond angles, polyhedral volumes, and twist angles for all analyzed samples. The volume of each Pb polyhedron was calculated using the software program VOLCAL (Hazen and Finger 1982). Minor substitution of Na and K ions in the control samples slightly affected the mean Pb1–O distances, resulting in the increase in the Pb1 polyhedral volume from 38.688  $\text{\AA}^3$  in Na-Pym to 38.729  $\text{\AA}^3$  in K-Pym. This is consistent with the smaller ionic radius of Na than that of K, which for ninefold

**TABLE 3.** Bond valence sums calculated for Pb, La, Na, and K in Pb1 and Pb2 structural sites in pyromorphite

	La-Na-Pym	Na-Pym	La-K-Pym	K-Pym
<b>Pb</b>				
Pb1	2.03	2.02	2.01	2.01
Pb2	1.98	1.97	1.99	1.98
<b>La</b>				
Pb1	2.20	–	2.16	–
Pb2	2.26	–	2.26	–
<b>Na</b>				
Pb1	0.85	0.84	–	–
Pb2	0.82	0.82	–	–
<b>K</b>				
Pb1	–	–	1.77	1.78
Pb2	–	–	1.86	1.86

Notes: Bond-valence parameters are taken from the studies by: Brown and Altermatt (1985) for  $K^+-Cl^-$ , Brese and O'Keeffe (1991) for  $Na^+-Cl^-$  and  $La^{3+}-Cl^-$ ; Hu (2007) for  $Pb^{2+}-Cl^-$ ; Gagné and Hawthorne (2015) for all cations  $-O^{2-}$ .

**TABLE 4.** Selected bond lengths (Å), bond angles (°), and twist angles (°) for all analyzed samples

	La-Na-Pym	Na-Pym	La-K-Pym	K-Pym
Pb1–O1 (×3)	2.572(3)	2.580(5)	2.581(4)	2.578(5)
–O2 (×3)	2.671(3)	2.672(5)	2.674(4)	2.675(5)
–O3 (×3)	2.877(3)	2.878(5)	2.881(5)	2.879(5)
Mean	2.707	2.710	2.712	2.711
Polyhedral volume (Å <sup>3</sup> )	38.515	38.688	38.777	38.729
Pb2–O1	3.065(3)	3.086(7)	3.079(4)	3.08619(11)
–O2	2.357(4)	2.359(7)	2.356(6)	2.352(6)
–O3 (×2)	2.630(3)	2.633(5)	2.625(4)	2.634(5)
–O3 (×2)	2.637(3)	2.637(5)	2.636(5)	2.635(5)
Cl (×2)	3.10891(18)	3.1109(6)	3.1131(2)	3.1103(3)
Mean	2.772	2.776	2.773	2.774
Polyhedral volume (Å <sup>3</sup> )	36.941	37.138	37.019	37.085
P–O1	1.528(4)	1.523(7)	1.519(6)	1.522(7)
–O2	1.555(4)	1.559(7)	1.557(6)	1.562(7)
–O3 (×2)	1.534(3)	1.538(5)	1.539(4)	1.537(5)
Mean	1.538	1.540	1.536	1.540
Polyhedral volume (Å <sup>3</sup> )	1.862	1.869	1.866	1.869
O1–P–O2	110.6(3)	110.5(4)	110.5(4)	110.3(4)
O1–P–O3 (×2)	112.19(16)	112.3(2)	112.3(2)	112.2(2)
O2–P–O3 (×2)	107.29(16)	107.2(3)	107.3(2)	107.4(2)
O3–P–O3	107.0(3)	107.0(4)	106.9(4)	107.0(4)
Twist angle	17.19	17.89	17.91	17.73

coordination are 1.24 and 1.55 Å, respectively (values taken from Shannon 1976). The mean Pb1–O distances for La-doped samples increased by 0.005 Å for La-K-Pym compared to those of La-Na-Pym, reflecting the polyhedral volume changes. The most sensitive bond for substitution was the Pb1–O1 bond, which varied from 2.572(3) Å (La-Na-Pym) to 2.581(4) Å (La-K-Pym). The Pb1 polyhedral volume for La-Na-Pym decreased by 0.173 Å<sup>3</sup> compared to the control sample, whereas the corresponding volume in La-K-Pym increased in comparison to the control sample by 0.048 Å<sup>3</sup>. This variation may be caused by the differences in ionic radii. In the case of Na and La substitutions for Pb, both substituting ions are smaller than Pb [ionic radii are: 1.216 Å ( $La^{3+}$ ) < 1.24 Å ( $Na^+$ ) < 1.35 Å ( $Pb^{2+}$ )], whereas in the case of K and La substitutions for Pb, the K ion is larger than Pb and the La ion is smaller [1.216 Å ( $La^{3+}$ ) < 1.35 Å ( $Pb^{2+}$ ) < 1.55 Å ( $K^+$ )]. However, the average ionic radii of La and K is very close to that of Pb, which may be the reason for the small volume change in this polyhedron compared to the control sample (only by 0.048 Å<sup>3</sup>). Variations in individual and mean interatomic distances in Pb1 polyhedron reflect the cumulative effect of both the amount of substitution and ionic radii of substituting ions.

Changes in the Pb1 polyhedron slightly affected the mean Pb2–O distances. The largest difference was visible for the

weakest bond, Pb2–O1, which was shorter in both the La-doped pyromorphites compared to the control samples. A similar trend was observed for the Pb2 polyhedral volume. Substitution in Pb1 did not affect the PO<sub>4</sub> tetrahedron, with volumes differing by only 0.007 Å<sup>3</sup>, which is within uncertainties. Moreover, all O–P–O angles within each PO<sub>4</sub> tetrahedron were identical in all refined structures.

Changes in distances also affected the unit-cell parameters and, consequently, their volumes (Table 2). The unit-cell parameter *c* appears to be more affected by the substitution and decreased in La-doped samples compared to the control samples. In La-Na-Pym, the unit-cell parameter *a* also decreased compared to the control sample. However, in La-K-Pym, *a* increased compared to K-Pym. This affected the volumes of the unit cell, and within the samples the smallest unit-cell volume, 630.680 Å<sup>3</sup>, was observed for La-Na-Pym. This is due to the substitution of two smaller ions ( $Na^+$  and  $La^{3+}$ ) for  $Pb^{2+}$ . In the La-K-Pym sample, the La content is lower than in La-Na-Pym, and the K ion is larger than Na, which resulted in an overall increase in the unit-cell volume.

## IMPLICATIONS

The restricted chemistry of synthetic analogs of La-doped pyromorphite allowed us to determine the effect of La substitution on the structure. From our single-crystal X-ray diffraction study, the following implications emerged. The mechanisms controlling La substitution in Pb-apatite are somewhat different from those in Ca-apatite. In both types of apatite, owing to the charge difference, heterovalent substitution of  $La^{3+}$  for  $Me^{2+}$  requires counter ions, which, in this case, were  $K^+$  and  $Na^+$ . However, in contrast to natural Ca-apatite, in Pb-apatite La occupies the Me1 site and not the Me2 site. This is at least the case in pyromorphites in which the counter ion is K or Na. It is possible that a greater size of Ca2 in Ca-chlorapatite diminishes the selectivity of this position for REE relative to that of Ca1 (Fleet et al. 2000). However, considering the present stage of knowledge, it is not possible to accurately compare the results obtained for pyromorphite with its calcium chlorapatite counterpart  $Ca_5(PO_4)_3Cl$  due to the difficulty in obtaining such apatite by simple synthesis from aqueous solutions. Therefore, it is difficult to clearly assess how much of this difference in substitution is due to the crystallization process and how much is due to a slight difference in structural properties, the influence of the lone-electron pair in  $Pb^{2+}$  ions, or the preference of Pb to occupy the Me2 site. It is not yet clear as to how the charges are balanced in REE substitutions in natural pyromorphite. Nevertheless, the magnitude of La substitution in the synthetic pyromorphites described here was larger than that reported in natural ones (see for example, Markl et al. 2014). This substitution model appears to be the model for all REE in Pb-apatite (or at least for all LREE).

Our preliminary tests with REE heavier than La indicate that the fractionation of REE during the crystallization of pyromorphite from aqueous solutions at ambient temperatures is nearly negligible. It is necessary to determine the structure of pyromorphite containing heavy REE (e.g., Yb, Lu) formed under identical conditions to determine the possible differences and similarities in the substitution mechanisms. However, only the determination of the structures of pyromorphite containing successively

(but separately) other REE, with different charge compensation mechanisms, will enable the determination of possible systematic similarities and discrepancies in the structures and substitution mechanisms depending on the ionic size and mass of the REE.

### ACKNOWLEDGMENTS AND FUNDING

Fernando Camara and an anonymous reviewer provided thoughtful reviews that are very gratefully acknowledged as they improved the present paper. This research was partly funded by the Polish NCN grant no. 2019/35/B/ST10/03379 and partly by program “Excellence initiative—research university” for the AGH University of Science and Technology.

### DECLARATION OF COMPETING INTERESTS

The authors declare that they have no known competing financial interests or personal relationships that could have appeared to influence the work reported in this paper.

### REFERENCES CITED

- Adler, H.H. (1964) Infrared spectra of phosphate minerals: Symmetry and substitutional effects in the pyromorphite series. *American Mineralogist. Journal of Earth and Planetary Materials*, 49, 1002–1015.
- Andersson, S.S., Wagner, T., Jonsson, E., Fusswinkel, T., and Whitehouse, M.J. (2019) Apatite as a tracer of the source, chemistry and evolution of ore-forming fluids: The case of the Olsersund-Djupedal REE-phosphate mineralisation, SE Sweden. *Geochimica et Cosmochimica Acta*, 255, 163–187, <https://doi.org/10.1016/j.gca.2019.04.014>.
- Baikie, T., Schreyer, M., Wei, F., Herrin, J.S., Ferraris, C., Brink, F., Topolska, J., Piltz, R.O., Price, J., and White, T.J. (2014) The influence of stereochemically active lone-pair electrons on crystal symmetry and twist angles in lead apatite-2H type structures. *Mineralogical Magazine*, 78, 325–345, <https://doi.org/10.1180/minmag.2014.078.2.07>.
- Bajda, T., Mozgawa, W., Manecki, M., and Flis, J. (2011) Vibrational spectroscopic study of mimetite–pyromorphite solid solutions. *Polyhedron*, 30, 2479–2485, <https://doi.org/10.1016/j.poly.2011.06.034>.
- Bartholomäi, G. and Klee, W.E. (1978) The vibrational spectra of pyromorphite, vanadinite and mimetite. *Spectrochimica Acta. Part A: Molecular Spectroscopy*, 34, 831–843, [https://doi.org/10.1016/0584-8539\(78\)80038-5](https://doi.org/10.1016/0584-8539(78)80038-5).
- Bauer, M. and Klee, W.E. (1993) The monoclinic-hexagonal phase transition in chlorapatite. *European Journal of Mineralogy*, 5, 307–316, <https://doi.org/10.1127/ejm/5/2/0307>.
- Belousova, E.A., Griffin, W.L., O’Reilly, S.Y., and Fisher, N.I. (2002) Apatite as an indicator mineral for mineral exploration: Trace-element compositions and their relationship to host rock type. *Journal of Geochemical Exploration*, 76, 45–69, [https://doi.org/10.1016/S0375-6742\(02\)00204-2](https://doi.org/10.1016/S0375-6742(02)00204-2).
- Bigi, A., Gandolfi, M., Gazzano, M., Ripamonti, A., Roveri, N., and Thomas, S.A. (1991) Structural modifications of hydroxyapatite induced by lead substitution for calcium. *Journal of the Chemical Society, Dalton Transactions: Inorganic Chemistry*, 11, 2883–2886, <https://doi.org/10.1039/dt9910002883>.
- Borisov, S.V. and Klevцова, R.F. (1963) The crystal structure of RE-Sr apatite. *Zhurnal Strukturnoi Khimii*, 4, 629–631.
- Botto, I.L., Barone, V.L., Castiglioni, J.L., and Schalamuk, I.B. (1997) Characterization of a natural substituted pyromorphite. *Journal of Materials Science*, 32, 6549–6553, <https://doi.org/10.1023/A:1018667428762>.
- Bouzari, F., Hart, C.J., Bissig, T., and Barker, S. (2016) Hydrothermal alteration revealed by apatite luminescence and chemistry: A potential indicator mineral for exploring covered porphyry copper deposits. *Economic Geology and the Bulletin of the Society of Economic Geologists*, 111, 1397–1410, <https://doi.org/10.2113/econgeo.111.6.1397>.
- Brese, N.E. and O’Keeffe, M. (1991) Bond-valence parameters for solids. *Acta Crystallographica*, B47, 192–197, <https://doi.org/10.1107/S0108768190011041>.
- Brown, I.D. and Altermatt, D. (1985) Bond-valence parameters obtained from a systematic analysis of the Inorganic Crystal Structure Database. *Acta Crystallographica*, B41, 244–247, <https://doi.org/10.1107/S0108768185002063>.
- Cockbain, A.G. and Smith, G.V. (1967) Alkaline-earth-rare-earth silicate and germanate apatites. *Mineralogical Magazine and Journal of the Mineralogical Society*, 36, 411–421, <https://doi.org/10.1180/minmag.1967.036.279.11>.
- Dai, Y. and Hughes, J.M. (1989) Crystal structure refinements of vanadinite and pyromorphite. *Canadian Mineralogist*, 27, 189–192.
- Elliot, J.C., Mackie, P.E., and Young, R.A. (1973) Monoclinic hydroxyapatite. *Science*, 180, 1055–1057.
- Fleet, M.E. and Pan, Y. (1995) Site preference of rare earth elements in fluorapatite. *American Mineralogist*, 80, 329–335.
- (1997a) Site preference of rare earth elements in fluorapatite: Binary (LREE+HREE)-substituted crystals. *American Mineralogist*, 82, 870–877, <https://doi.org/10.2138/am-1997-9-1004>.
- (1997b) Rare earth elements in apatite: Uptake from H<sub>2</sub>O-bearing phosphate fluoride melts and the role of volatile components. *Geochimica et Cosmochimica Acta*, 61, 4745–4760, [https://doi.org/10.1016/S0016-7037\(97\)00292-5](https://doi.org/10.1016/S0016-7037(97)00292-5).
- Fleet, M.E., Liu, X., and Pan, Y. (2000) Rare-earth elements in chlorapatite [Ca<sub>10</sub>(PO<sub>4</sub>)<sub>6</sub>Cl<sub>2</sub>]: Uptake, site preference, and degradation of monoclinic structure. *American Mineralogist*, 85, 1437–1446, <https://doi.org/10.2138/am-2000-1012>.
- Fleet, M.E., Liu, X., and King, P.L. (2004) Accommodation of the carbonate ion in apatite: An FTIR and X-ray structure study of crystals synthesized at 2–4 GPa. *American Mineralogist*, 89, 1422–1432, <https://doi.org/10.2138/am-2004-1009>.
- Frost, R.L. and Palmer, S.J. (2007) A Raman spectroscopic study of the phosphate mineral pyromorphite Pb<sub>5</sub>(PO<sub>4</sub>)<sub>3</sub>Cl. *Polyhedron*, 26, 4533–4541, <https://doi.org/10.1016/j.poly.2007.06.004>.
- Gagné, O.C. and Hawthorne, F.C. (2015) Comprehensive derivation of bond-valence parameters for ion pairs involving oxygen. *Acta Crystallographica*, B71, 562–578, <https://doi.org/10.1107/S2052520615016297>.
- Gu, T., Qin, S., and Wu, X. (2020) Thermal behavior of pyromorphite (Pb<sub>10</sub>(PO<sub>4</sub>)<sub>6</sub>Cl<sub>2</sub>): In situ high temperature powder X-ray diffraction study. *Crystals*, 10, 1070, <https://doi.org/10.3390/cryst10121070>.
- Harlov, D.E. (2015) Apatite: A fingerprint for metasomatic processes. *Elements (Quebec)*, 11, 171–176, <https://doi.org/10.2113/gselements.11.3.171>.
- Hazen, R.M. and Finger, L.W. (1982) *Comparative Crystal Chemistry: Temperature, pressure, composition, and the variation of crystal structure*, 248 p. Wiley.
- Hovis, G., Abraham, T., Hudacek, W., Wildermuth, S., Scott, B., Altomare, C., Medford, A., Conlon, M., Morris, M., Leaman, A., and others. (2015) Thermal expansion of F-Cl apatite crystalline solutions. *American Mineralogist*, 100, 1040–1046, <https://doi.org/10.2138/am-2015-5176>.
- Hu, S.-Z. (2007) A new approach to bond valence parameters for Pb(II)-halide bonds. *Wuli Huaxue Xuebao*, 23, 786–789.
- Hughes, J.M., Cameron, M., and Mariano, A.N. (1991) Rare-earth-element ordering and structural variations in natural rare-earth-bearing apatites. *American Mineralogist*, 76, 1165–1173.
- Jarosewich, E. and Boatner, L.A. (1991) Rare-earth element reference samples for electron microprobe analysis. *Geostandards and Geoanalytical Research*, 15, 397–399, <https://doi.org/10.1111/j.1751-908X.1991.tb00115.x>.
- Jonsson, E., Harlov, D.E., Majka, J., Högdahl, K., and Persson-Nilsson, K. (2016) Fluorapatite-monazite-allanite relations in the Grängesberg apatite-iron oxide ore district, Bergslagen, Sweden. *American Mineralogist*, 101, 1769–1782, <https://doi.org/10.2138/am-2016-5655>.
- Kampf, A.R. and Housley, R.M. (2011) Fluorophosphohedyphane, Ca<sub>2</sub>Pb<sub>3</sub>(PO<sub>4</sub>)<sub>3</sub>F, the first apatite supergroup mineral with essential Pb and F. *American Mineralogist*, 96, 423–429, <https://doi.org/10.2138/am.2011.3586>.
- Kampf, A.R., Steele, I.M., and Jenkins, R.A. (2006) Phosphohedyphane, Ca<sub>2</sub>Pb<sub>3</sub>(PO<sub>4</sub>)<sub>3</sub>Cl, the phosphate analog of hedyphane: Description and crystal structure. *American Mineralogist*, 91, 1909–1917, <https://doi.org/10.2138/am.2006.2268>.
- Kim, J.Y., Fenton, R.R., Hunter, B.A., and Kennedy, B.J. (2000) Powder diffraction studies of synthetic calcium and lead apatites. *Australian Journal of Chemistry*, 53, 679–686, <https://doi.org/10.1071/CH00060>.
- Knyazev, A.V., Bulanov, E.N., and Korokin, V.Z. (2015) Thermal expansion of solid solutions in apatite binary systems. *Materials Research Bulletin*, 61, 47–53, <https://doi.org/10.1016/j.materresbull.2014.09.089>.
- Kwaśniak-Kominek, M., Manecki, M., Matusik, J., and Lempart, M. (2017) Carbonate substitution in lead hydroxyapatite Pb<sub>5</sub>(PO<sub>4</sub>)<sub>3</sub>OH. *Journal of Molecular Structure*, 1147, 594–602, <https://doi.org/10.1016/j.molstruc.2017.06.111>.
- Laperche, V., Logan, T.J., Gaddam, P., and Traina, S.J. (1997) Effect of apatite amendments on plant uptake of lead from contaminated soil. *Environmental Science & Technology*, 31, 2745–2753, <https://doi.org/10.1021/es961011o>.
- Levitt, S.R. and Condrate, R.A. Sr. (1970) The vibrational spectra of lead apatites. *American Mineralogist. Journal of Earth and Planetary Materials*, 55, 1562–1575.
- Ma, Q.Y., Traina, S.J., Logan, T.J., and Ryan, J.A. (1993) In situ lead immobilization by apatite. *Environmental Science & Technology*, 27, 1803–1810, <https://doi.org/10.1021/es00046a007>.
- Ma, Q.Y., Logan, T.J., and Traina, S.J. (1995) Lead immobilization from aqueous solutions and contaminated soils using phosphate rocks. *Environmental Science & Technology*, 29, 1118–1126, <https://doi.org/10.1021/es00004a034>.
- Mackie, P.E. and Young, R.A. (1973) Location of Nd dopant in fluorapatite, Ca<sub>5</sub>(PO<sub>4</sub>)<sub>3</sub>F: Nd. *Journal of Applied Crystallography*, 6, 26–31, <https://doi.org/10.1107/S0021889873008009>.
- Mackie, P.E., Elliot, J.C., and Young, R.A. (1972) Monoclinic structure of synthetic Ca<sub>5</sub>(PO<sub>4</sub>)<sub>3</sub>Cl, chlorapatite. *Acta Crystallographica*, B28, 1840–1848, <https://doi.org/10.1107/S0567740872005114>.
- Manecki, M. (2019) Lead in Water and Soil: Speciation, Toxicity, and Treatment Technologies. In P.A. Maurice, Ed., *Encyclopedia of Water: Science, Technology, and Society*, p. 1713–1727. Wiley.
- Manecki, M., Maurice, P.A., and Traina, S.J. (2000) Kinetics of aqueous Pb reaction with apatites. *Soil Science*, 165, 920–933, <https://doi.org/10.1097/00010694-200012000-00002>.

- Maneck, M., Kwaśniak-Kominek, M., Majka, J.M., and Rakovan, J. (2020) Model of interface-coupled dissolution-precipitation mechanism of pseudomorphic replacement reaction in aqueous solutions based on the system of cerussite  $\text{PbCO}_3$ -pyromorphite  $\text{Pb}_5(\text{PO}_4)_3\text{Cl}$ . *Geochimica et Cosmochimica Acta*, 289, 1–13, <https://doi.org/10.1016/j.gca.2020.08.015>.
- Markl, G., Marks, M.A., Holzäpfel, J., and Wenzel, T. (2014) Major, minor, and trace element composition of pyromorphite-group minerals as recorder of supergene weathering processes from the Schwarzwald mining district, SW Germany. *American Mineralogist*, 99, 1133–1146, <https://doi.org/10.2138/am.2014.4789>.
- Mayer, I. and Swissa, S. (1985) Lead and strontium phosphate apatites substituted by rare earth and silver ions. *Journal of the Less Common Metals*, 110, 411–414, [https://doi.org/10.1016/0022-5088\(85\)90350-9](https://doi.org/10.1016/0022-5088(85)90350-9).
- Mayer, I., Semadja, A., and Weiss, V. (1980) Lead phosphate apatites substituted by rare earth, sodium, and potassium ions. *Journal of Solid State Chemistry*, 34, 223–229, [https://doi.org/10.1016/0022-4596\(80\)90225-X](https://doi.org/10.1016/0022-4596(80)90225-X).
- Newby, H.P. (1981) Rare-earth elements in pyromorphite-group minerals. Ph.D. dissertation, University of London Reactor Centre, Department of Mechanical Engineering, Imperial College of Science and Technology.
- Nriagu, J.O. (1974) Lead orthophosphates—IV Formation and stability in the environment. *Geochimica et Cosmochimica Acta*, 38, 887–898, [https://doi.org/10.1016/0016-7037\(74\)90062-3](https://doi.org/10.1016/0016-7037(74)90062-3).
- Okudera, H. (2013) Relationships among channel topology and atomic displacements in the structures of  $\text{Pb}_5(\text{BO}_3)_2\text{Cl}$  with B = P (pyromorphite), V (vanadinite), and As (mimetite). *American Mineralogist*, 98, 1573–1579, <https://doi.org/10.2138/am.2013.4417>.
- O'Sullivan, G.J., Chew, D.M., Morton, A.C., Mark, C., and Henrichs, I.A. (2018) An integrated apatite geochronology and geochemistry tool for sedimentary provenance analysis. *Geochemistry, Geophysics, Geosystems*, 19, 1309–1326, <https://doi.org/10.1002/2017GC007343>.
- Pan, Y. and Fleet, M.E. (2002) Compositions of the apatite-group minerals: Substitution mechanisms and controlling factors. *Reviews in Mineralogy and Geochemistry*, 48, 13–49, <https://doi.org/10.2138/rmg.2002.48.2>.
- Papke, J.J., Jensen, M., Shearer, C.K., Simon, S.B., Walker, R.J., and Laul, J.C. (1984) Apatite as a recorder of pegmatite petrogenesis. *Geological Society of America Abstracts with Programs*, 16, 617.
- Pasero, M., Kampf, A.R., Ferraris, C., Pekov, I.V., Rakovan, J., and White, T.J. (2010) Nomenclature of the apatite supergroup minerals. *European Journal of Mineralogy*, 22, 163–179, <https://doi.org/10.1127/0935-1221/2010/0022-2022>.
- Rakovan, J. and Reeder, R.J. (1996) Intracrystalline Rare Earth Element distributions in apatite: Surface structural influences on incorporation during growth. *Geochimica et Cosmochimica Acta*, 60, 4435–4445, [https://doi.org/10.1016/S0016-7037\(96\)00244-X](https://doi.org/10.1016/S0016-7037(96)00244-X).
- Ronsbo, J.G. (1989) Coupled substitutions involving REEs and Na and Si in apatites in alkaline rocks from the Ilimaussaq intrusion, South Greenland, and the petrological implications. *American Mineralogist*, 74, 896–901.
- Rouse, R.C., Dunn, P.J., and Peacor, D.R. (1984) Hedyphane from Franklin, New Jersey and Långban, Sweden: Cation ordering in an arsenate apatite. *American Mineralogist*, 69, 920–927.
- Sha, L.K. and Chappell, B.W. (1999) Apatite chemical composition, determined by electron microprobe and laser-ablation inductively coupled plasma mass spectrometry, as a probe into granite petrogenesis. *Geochimica et Cosmochimica Acta*, 63, 3861–3881, [https://doi.org/10.1016/S0016-7037\(99\)00210-0](https://doi.org/10.1016/S0016-7037(99)00210-0).
- Shannon, R.D. (1976) Revised effective ionic radii and systematic studies of interatomic distances in halides and chalcogenides. *Acta Crystallographica*, 32, 751–767, <https://doi.org/10.1107/S0567739476001551>.
- Sheldrick, G.M. (2015) Crystal structure refinement with SHELXL. *Acta Crystallographica*, C71, 3–8, <https://doi.org/10.1107/S2053229614024218>.
- Tang, P., Zhou, Y.C., and Xie, Z.M. (2013) Immobilization of heavy metals in sludge using phosphoric acid and monobasic calcium phosphate. *Journal of Zhejiang University. Science A*, 14, 177–186, <https://doi.org/10.1631/jzus.A1200263>.
- Vignoles, M., Bonel, G., Holcomb, D.W., and Young, R.A. (1988) Influence of preparation conditions on the composition of type B carbonated hydroxyapatite and on the localization of the carbonate ions. *Calcified Tissue International*, 43, 33–40, <https://doi.org/10.1007/BF02555165>.
- White, T., Ferraris, C., Kim, J., and Madhavi, S. (2005) Apatite—an adaptive framework structure. *Reviews in Mineralogy and Geochemistry*, 57, 307–401, <https://doi.org/10.2138/rmg.2005.57.10>.
- Zhang, L., Chen, Z., Wang, F., and Zhou, T. (2021) Apatite geochemistry as an indicator of petrogenesis and uranium fertility of granites: A case study from the Zhuguangshan batholith, South China. *Ore Geology Reviews*, 128, 103886, <https://doi.org/10.1016/j.oregeorev.2020.103886>.

MANUSCRIPT RECEIVED JUNE 18, 2022

MANUSCRIPT ACCEPTED FEBRUARY 4, 2023

ACCEPTED MANUSCRIPT ONLINE FEBRUARY 16, 2023

MANUSCRIPT HANDLED BY YASSIR A. ABDU

### Endnote:

<sup>1</sup>Deposit item AM-23-128664. Online Materials are free to all readers. Go online, via the table of contents or article view, and find the tab or link for supplemental materials.